Molecular Genetics and Metabolism Reports 41 (2024) 101165

Contents lists available at ScienceDirect

Molecular Genetics and Metabolism Reports

journal homepage: www.elsevier.com/locate/ymgmr

Homozygous *slc25a20* zebrafish mutant reveals insights into carnitine-acylcarnitine translocase deficiency pathogenesis

Ryuichi Hishida [a], Kohei Ishiguro [a], Tomoyuki Yamanaka [a], Shinya Toyokuni [b,c], Hideaki Matsui [a,*]

[a] Department of Neuroscience of Disease, Brain Research Institute, Niigata University, Niigata 951-8585, Japan
[b] Department of Pathology and Biological Responses, Nagoya University Graduate School of Medicine, Nagoya 466-8550, Japan
[c] Center for Low-temperature Plasma Sciences, Nagoya University, Furo-cho, Chikusa-ku, Nagoya 464-8603, Japan

ARTICLE INFO

Keywords:
Zebrafish
slc25a20
Carnitine-acylcarnitine translocase deficiency
Hypertrophied
Lipid storage myopathy
Fatty liver

ABSTRACT

The *SLC25A20* gene encodes carnitine-acylcarnitine translocase (CACT), facilitating the transport of long-chain acylcarnitine required for energy production via β-oxidation into the mitochondria. Loss-of-function mutations in this gene lead to CACT deficiency, a rare autosomal recessive disorder of fatty acid metabolism characterized by severe symptoms including cardiomyopathy, hepatic dysfunction, rhabdomyolysis, hypoketotic hypoglycemia, and hyperammonemia, often resulting in neonatal mortality. Here, we utilized CRISPR/Cas9 gene editing to isolate *slc25a20* mutant zebrafish. Homozygous mutants displayed significant lethality, with the majority succumbing before reaching maturity. However, we identified a notably rare homozygous individual that survived into adulthood, prompting a histological examination. Firstly, we observed adipose tissue accumulation at various sites in the homozygous mutant. The mutant heart exhibited hypertrophy, along with degenerated myocardial and muscle cells containing numerous eosinophilic nuclei. Additionally, we found no large oil droplet vacuoles in the mutant liver; however, the hepatocytes displayed numerous small vacuoles resembling lipid droplets. Iron deposition was evident in the spleen and parts of the liver. Overall, our *slc25a20* zebrafish mutant displayed tissue pathologies analogous to human CACT deficiency, suggesting its potential as a pathological model contributing to the elucidation of pathogenesis and the improvement/development of therapies for CACT deficiency.

1. Introduction

Carnitine-acylcarnitine translocase (CACT) deficiency is a rare autosomal recessive disorder of fatty acid metabolism characterized by severe symptoms [1–4]. CACT is a membrane antiporter protein consisting of 301 amino acids, encoded by the solute carrier family 25 member 20 (*SLC25A20*) gene [5–7]. It plays a crucial role in the carnitine cycle by facilitating the transport of L-carnitine out of the mitochondrial inner membrane while simultaneously transporting long-chain acylcarnitine into the inner membrane [8]. Long-chain acylcarnitine transported into the mitochondria is then converted to acyl CoA, utilized for energy production via β-oxidation [9]. Deficiency of CACT leads to reduced energy production from long-chain fatty acids, endogenous toxicity due to accumulation of long-chain acylcarnitine, and thus impaired organ function, particularly in the heart, skeletal muscle, and liver, where β-oxidation is active.

CACT deficiency manifests in two phenotypes: a severe neonatal-onset form, predominant among patients, and a late-onset form [2,4,10,11]. Patients with the late-onset form typically exhibit milder symptoms, while those with the neonatal-onset form experience severe symptoms that often develop within 2 days of birth, including hyperammonaemia, cardiomyopathy or arrhythmias, liver dysfunction with hepatomegaly, and skeletal muscle damage or rhabdomyolysis [2,11], leading to sudden death in the neonatal period in the majority of the cases [2,10–13]. Cases have been reported of patients, including those with the severe form of the disease, who survived for more than a year with accurate diagnosis and treatment centered on dietary management [11,14]. This suggests that a more detailed analysis of the disease and the search for optimal treatment strategies could improve outcomes. However, progress remains limited by the small number of reported cases (89 neonatal-onset cases and 14 late-onset cases as of 2022) [4] and the lack of an appropriate pathological model.

* Corresponding author at: Department of Neuroscience of Disease, Brain Research Institute, Niigata University, 1-757, Asahimachidori, Niigata 951-8585, Japan.
E-mail address: hide0729@bri.niigata-u.ac.jp (H. Matsui).

https://doi.org/10.1016/j.ymgmr.2024.101165
Received 28 June 2024; Received in revised form 15 November 2024; Accepted 18 November 2024

Zebrafish, a vertebrate model organism, is useful for studying human disease pathogenesis due to not only ethical considerations, but also ease of genetic manipulation and high fecundity allowing large-scale experiments [15–17]. In this study, we generated a *slc25a20* mutant zebrafish to elucidate the function of the *slc25a20* gene and the pathogenesis of CACT deficiency. While the homozygous mutants exhibited high lethality with few surviving to adulthood, we identified a rare adult survivor and conducted histopathological analyses to examine tissue phenotypes, revealing similarities to observed human phenotypes.

2. Materials and methods

2.1. Ethics approval

All animal experiments were performed in compliance with the protocol reviewed by the Institutional Animal Care and Use Committee and approved by the President of Niigata University (#SA01244).

2.2. Zebrafish husbandry

Zebrafish (AB strain) were raised and maintained under a 14-h light/10-h dark cycle at 28 °C following standard protocols. Fish were fed brine shrimp at 9:00 a.m. and powdered feed (Kyorin, Himeji, Japan) at 12:00 p.m. [18]

2.3. CRISPR/Cas9 genome editing

The setup for the microinjection was described previously [11]. To generate *slc25a20* -mutant zebrafish, a mixture of guide RNA (target sequence: GGAGAAGTCGCGCAGTACGCCGG, 25 ng/μl), Cas9 protein (0.6 μg/μl; New England Biolabs, Ipswich, MA) and phenol red (2 %) was microinjected into one-cell-stage fish embryos as previously described [19,20]. F1 and subsequent generations were genotyped as follows. A small portion of the caudal fin was collected from each fish, and genomic DNA was extracted using the KANEKA Easy DNA Extraction Kit version 2 (Kaneka Corp., Japan). The DNA was used as a template for PCR amplification of the region surrounding the mutation site (forward primer: TCTGTGTGTGCGTGACCTTT; reverse primer: GGCCAGTGTTTTCTTGAAGC). Amplified DNA fragments were sequenced by Eurofins Genomics (Tokyo, Japan) at the mutation site using the forward primer to confirm genotypes.

2.4. Transcript expression analysis

The relative expression levels across each organ were compared based on transcripts per million (TPM) as follows. RNA sequencing data for multiple adult zebrafish tissues are publicly available at the National Center for Biotechnology Information (NCBI) Gene Expression Omnibus (https://www.ncbi.nlm.nih.gov/geo/query/acc.cgi?acc=GSE171906). Data for nine organs (brain, heart, intestine, liver, muscle, skin, spleen, tail, and testis) were obtained, with three biological replicates per organ (27 samples total, from GSM5237120 to GSM5237146). The TPM values were consolidated, and the mean and standard error of the mean were calculated.

In situ hybridization was done as follows. Partial *slc25a20* cDNA sequence of zebrafish was synthesized by Eurofins Genomics (Tokyo, Japan) and was subcloned into T-Vector pMD20 (TakaraBio, Kusatsu, Japan). Digoxigenin (DIG)-labeled riboprobes were synthesized using the DIG RNA labeling kit (Roche Diagnostics, Basel, Switzerland) following the manufacturer's instructions. Subsequent mRNA in situ hybridization was performed as previously described [21]. In addition to the *slc25a20* gene, we conducted in situ hybridization experiments simultaneously on two other unrelated genes. Each of the three antisense probes produced distinct and characteristic signal patterns, confirming that the results were unlikely to be due to non-specific signals.

2.5. Histological experiments

Mutant and WT zebrafish were euthanized by immersion in water from the breeding system containing 0.1 % Tricaine. Entire bodies with a small incision in the abdomen were fixed in 4 % paraformaldehyde at 4 °C overnight, followed by decalcification in ethylenediaminetetraacetic acid (EDTA) solution. After a series of ethanol and xylene washes, the specimens were embedded in paraffin and sectioned into 3-μm sections. Hematoxylin-eosin (HE) staining, azan staining, and Prussian blue staining were performed using standard protocols.

3. Results

3.1. Generation of slc25a20 mutant zebrafish

To gain deeper insights into the pathogenesis of CACT deficiency and the role of *SLC25A20*, we generated zebrafish with a mutation in the *slc25a20* gene. Injection of guide RNA along with Cas9 protein into one-cell stage fish embryos led to the production of F0 mosaic mutants. Subsequently, F0 mosaic mutants were bred with wildtype AB zebrafish to produce a heterozygous mutant F1 generation. Upon genotyping this cohort, we identified a mutant harboring a 2-bp insertion at the target site within exon 2 of the *slc25a20* gene (Fig. 1A, NM_200859.1: c.152_153insCA p.(Ala52Thrfs*31) in HGVS c. and p. nomenclature). The resultant frameshift caused by this insertion is predicted to yield a protein in which the 51st tyrosine residue of the Slc25a20 protein is followed by an unrelated 30-amino acid sequence (Fig. 1B&C). This mutation removes 83.0 % of the Slc25a20 protein, which exhibits high conservation across various vertebrates throughout its entire length (of the 300 amino acid zebrafish protein, 241 amino acids are identical to mice (80.3 %) and 243 amino acids to humans (81.0 %)). Moreover, this mutation leads to the loss of many amino acid residues critical for transport activity, as reported in previous studies [7,22]. These findings strongly suggest that the function of the *slc25a20* gene is disrupted in the zebrafish mutant.

3.2. Expression of slc25a20 gene

We examined the spatial and temporal expression patterns of the *slc25a20* gene. RNA sequencing analysis profiling transcript expression levels across adult zebrafish tissues (data obtained from the public database, https://www.ncbi.nlm.nih.gov/geo/query/acc.cgi?acc=GSE171906) revealed its widespread expression, with notably elevated levels observed in the brain, heart, intestine, liver, and skin (Fig. 2A). Furthermore, we corroborated this ubiquitous expression pattern through in situ hybridization of *slc25a20* mRNA in juvenile fish as well (Fig. 2B). The *slc25a20* gene, involved in mitochondrial energy metabolism, exhibited ubiquitous expression across various organs in juvenile and adult zebrafish, as expected from its biological role.

3.3. Histological analysis of the slc25a20 mutant

To analyze the phenotype of the *slc25a20* mutant, F1 heterozygous animals were bred through in-crossing to generate homozygous fish. At approximately 1.5–3.5 months of age, 48 F2 progeny were genotyped, revealing only one homozygous mutant (homozygous (n = 1, 2 %); heterozygous (n = 34, 71 %); WT (n = 13, 27 %)), indicating strong lethality in homozygous fish. However, despite its lethality, the appearance of the surviving case of the homozygous mutant was not particularly strikingly abnormal (Fig. 3A). Upon close observation, the mutant exhibited slightly awkward swimming behavior and a slightly larger body size compared to the wild type. Specifically, the standard length (SL) [23] of the mutant was 24.5 mm, and the height at the anterior of the anal fin (HAA) [23] was 4.9 mm. In contrast, the average wild-type fish from the F2 progeny, as shown in Fig. 3A, had an SL of 19.2 mm and an HAA of 3.6 mm. We conducted a thorough search for

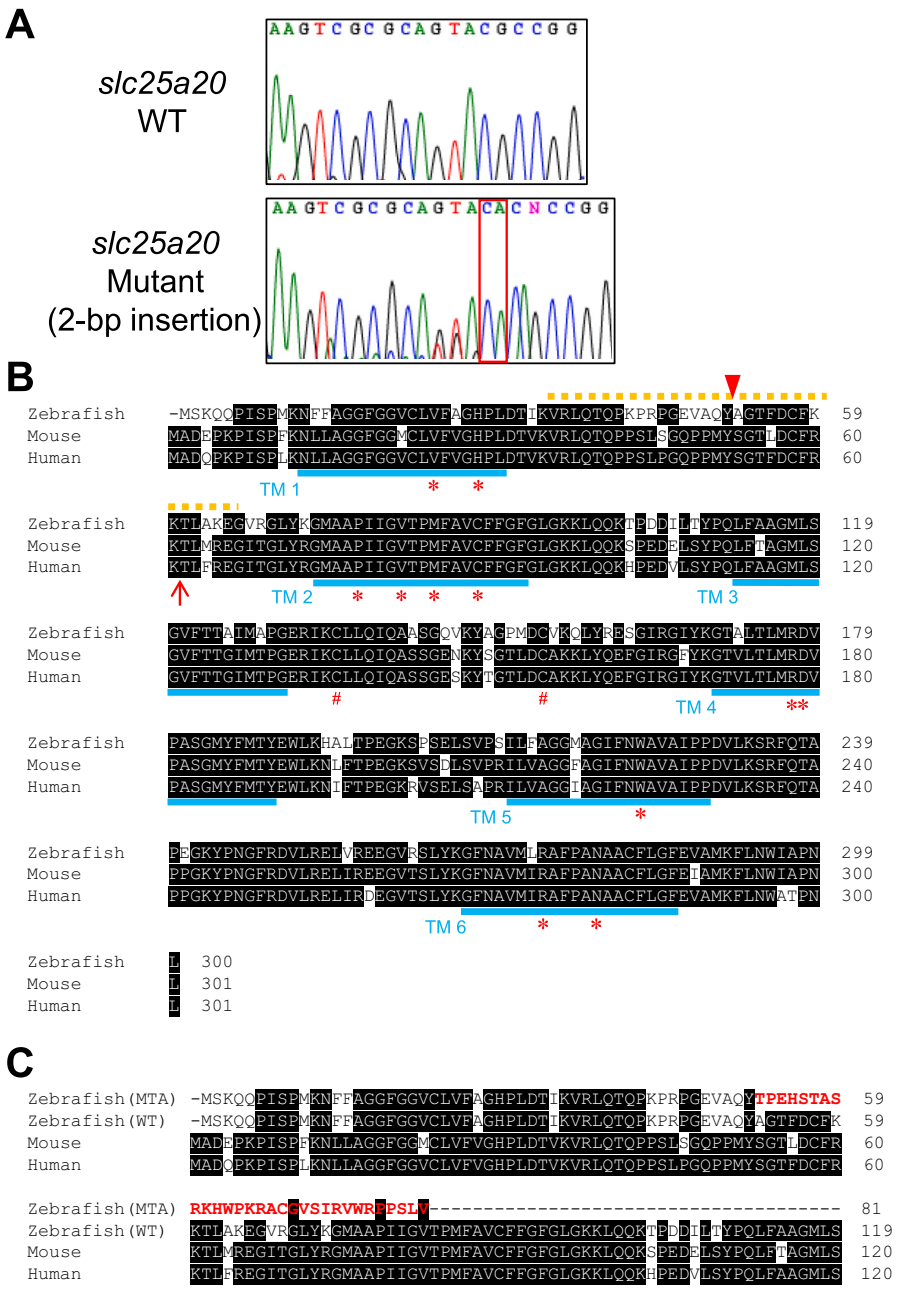

Fig. 1. Generation of *slc25a20* mutant zebrafish. (A) Sequences of wild-type (WT) and *slc25a20* mutant fish are shown. The red square indicates the insertion with a 2-base pair addition. The N (G or A) after the insertion site represents a genetic polymorphism. (B) Protein sequence of zebrafish Slc25a20. Comparison of the amino acid sequence of SLC25A20 among *D. rerio*, *M. musculus*, and humans. Sequence alignment was conducted using Clustal Omega (https://www.ebi.ac.uk/jdispatcher/msa/clustalo) [58]. Shaded residues indicate conserved amino acids. The red arrowhead indicates the position of the insertion mutation in *D. rerio*, isolated in this study. The orange dotted line indicates the site encoded by exon 2 in zebrafish. Blue bars indicate the positions of the 6 presumed transmembrane domains [5]. Red asterisks and sharps indicate the amino acid residues involved in binding substrate molecules and in cell redox sensing and control, respectively [7,22]. The red arrow indicates the position of the frameshift mutation (p.Lys61fs) found in a severely ill patient [27,35]. (C) Protein sequence of zebrafish Slc25a20 (MTA) and its comparison of the amino acid sequence. The red bold characters indicate the unrelated 30-amino acid sequence after the frameshift.

similar individuals with awkward movements, not only among the 48 genotyped F2 offspring but also among over 100 additional F2 offspring. However, no other such individuals were identified.

To investigate the morphological phenotype of the *slc25a20* mutant, we euthanized both the homozygous mutant and a simultaneously obtained wild type fish (both male) and conducted hematoxylin and eosin (HE) staining on 3-μm sections (Fig. 3B). Initially, we examined the coelomic cavity in general and observed a significantly higher presence of mature adipose tissue in the mutant compared to the wild type (Fig. 3C). Substantial amounts of adipose tissue were noted in various locations within the mutant, including between internal organs such as the liver and intestine (Fig. 3C4), adjacent to the testes (Fig. 3C5), and external to the coelomic cavity (Fig. 3C6). These observations indicated an abnormal accumulation of mature adipose tissue in the homozygous mutant.

Given the prevalence of severe heart failure in many patients with CACT deficiency [2,11,12], we examined the heart of the mutant for morphological abnormalities (Fig. 4). In terms of the overall organ shape, the heart of the mutant was noticeably hypertrophied compared to that of wild type fish (Fig. 4A1, A4). Upon examination of the internal

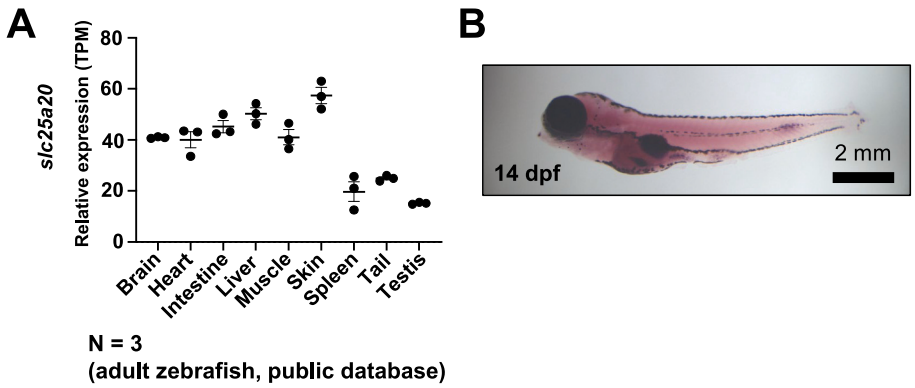

Fig. 2. Transcript expression profile of the *slc25a20* gene. (A) RNA sequence analysis reveals the ubiquitous expression of the gene in adult fish (data obtained from the public database, https://www.ncbi.nlm.nih.gov/geo/query/acc.cgi?acc=GSE171906). The relative expression levels of each organ are compared on TPM (transcripts per million) basis. (B) In situ hybridization of *slc25a20* mRNA demonstrates its ubiquitous expression in 14-day-old fry.

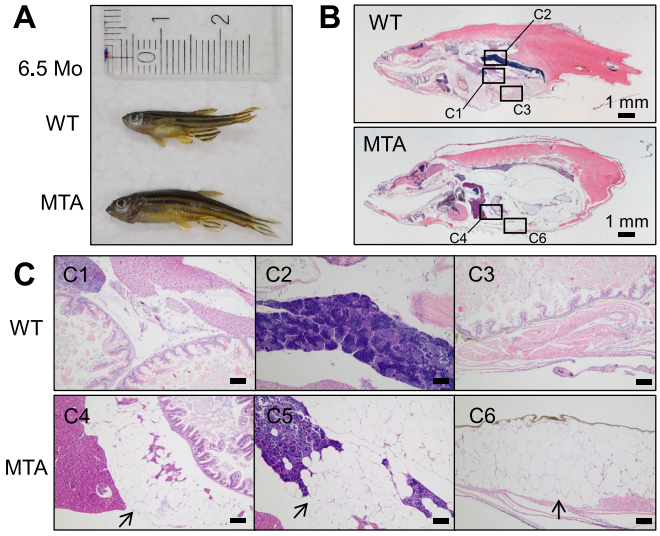

Fig. 3. Adipose tissue accumulation inside and outside the coelomic cavity of the *slc25a20* mutant. (A) Appearance of zebrafish used for tissue analysis. (B) Representative hematoxylin and eosin (HE) staining of 3-μm paraffin sections from the individuals showing a cross-section of the whole body. Squares correspond to the magnified regions shown in the following images. (C) Marked accumulation of adipose tissue in the mutant (C4–6) compared to the wild-type fish (C1–3). The images between the liver and the intestine (C1, C4), near the testes (C2, C4), and just outside of the coelomic cavity (C3, C6) are shown. Image C5 was taken from a different section than the one in *B*. The back arrows indicate abnormal accumulation of adipose tissue. Scale bar, 100 μm.

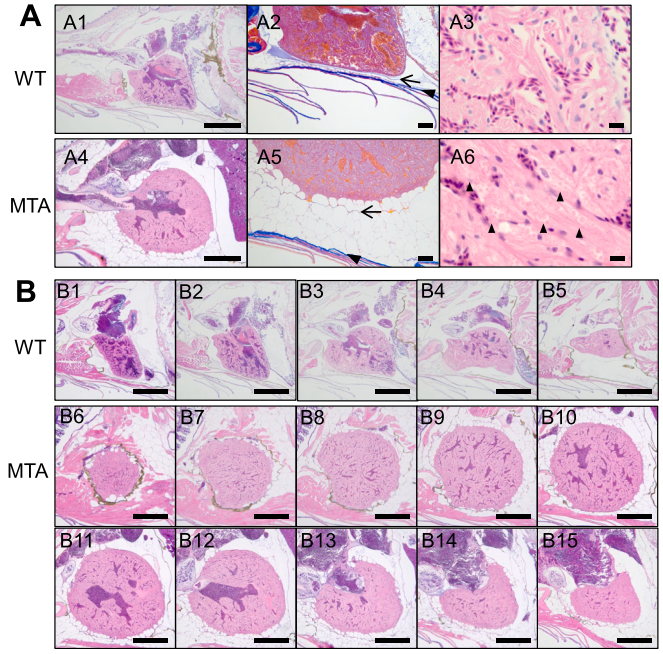

Fig. 4. Hypertrophy and abnormal histology observed in the heart of the *slc25a20* mutant. (A) Representative cardiac images of the wild-type fish (A1–3) and the mutant (A4–6). (A1, A4) Low-magnification images of the hearts from hematoxylin and eosin (HE)-stained paraffin sections. Scale bars, 0.5 mm. (A2, A5) Images of azan-stained paraffin sections adjacent to those in A1 and A4. Arrowhead and arrow indicate the connective tissue layer just inside the ventral skin and the coelomic membrane, respectively. Scale bars, 100 μm. (A3, A6) High-magnification images of the ventricles from HE-stained paraffin sections. The back arrowheads indicate eosin-negative membranes surrounding eosin-positive nuclei. Scale bars, 10 μm. (B) Cardiac images of serial HE-stained sections of the wild-type fish (B1–5) and the mutant (B6–15). The positions of the A1 and A4 sections are between the B2 and B3 sections and between the B12 and B13 sections, respectively. The distance between the sections is approximately 30 μm. Scale bar, 0.5 mm.

structure, the ventricle of wild-type fish exhibited myocardial cells arranged in a typical trabecular meshwork with blood filling the interstitial spaces [24]. Conversely, the ventricle of the mutant was densely packed with cardiomyocytes and displayed a reduced proportion of blood-containing space. This characteristic of myocardial packing was consistent across various sections of the heart and was identified as an abnormality in the mutant heart (Fig. 4B). Azan-stained sections revealed the absence of adipose tissue both inside and outside the coelomic membrane in wild type fish (Fig. 4 A2). In contrast, a substantial amount of adipose tissue was observed on either side of the membrane in the mutant, with fat cells infiltrating through the organ boundaries and adhering to the heart surface (Fig. 4A5). Examination of myocardial fibers at high magnification revealed some eosin-negative vacuoles that seemed to be oil droplets and numerous particles within cardiomyocytes throughout the ventricle of the mutant, a feature not seen in wild type fish (Fig. 4A3, A6). Stained images of some of these particles exhibited eosin-negative membranes surrounding eosin-positive nuclei. These findings indicate that the mutant heart mimicked the cardiac disease of patients with human CACT deficiency.

Next, we conducted a histological examination of the skeletal muscle of the mutant to identify morphological abnormalities (Fig. 5). Particularly in the muscles adjacent to the skin and around the myoseptum of the mutant, we found a significant amount of adipose tissue and the muscle cells in the vicinity had sarcomere structure disrupted and degenerated (Fig. 5A). Additionally, we observed numerous particles

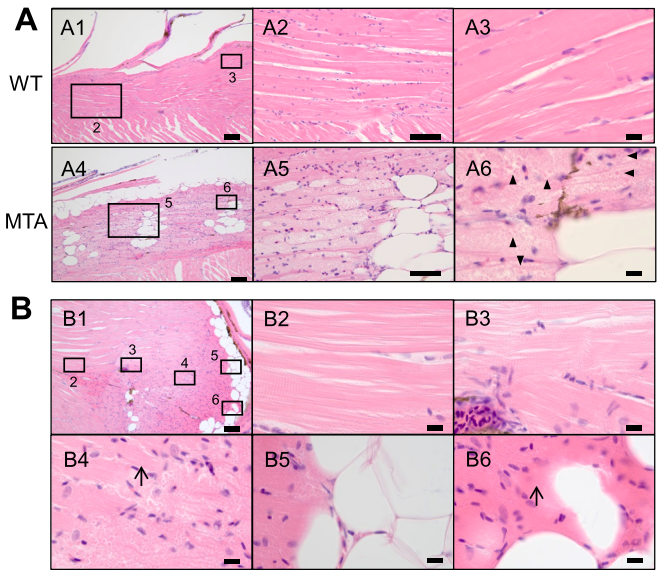

Fig. 5. Adipose accumulation and degeneration observed in the skeletal muscle of the *slc25a20* mutant. (A) Representative images of the skeletal muscle from hematoxylin and eosin (HE)-stained paraffin sections of the wild-type fish (A1–3) and the mutant (A4–6). (A1, A4) Low-magnification images of the skeletal muscles in the dorsal trunk. Squares correspond to the magnified regions shown in the following images. Scale bars, 100 μm. (A2, A5) Magnified images. Scale bars, 50 μm. (A3, A6) High-magnification images. The back arrowheads indicate eosin-negative membranes surrounding eosin-positive nuclei. Scale bars, 10 μm. (B) Representative images of the skeletal muscle in the tail region near the trunk from the HE-stained paraffin section of the mutant (the same section as in Fig. 3B). The body surface of the tail was sloped, so in the cut surface of this section, the tissue is closer to the skin from the left side to the right side. (B1) Low-magnification image. Squares correspond to the magnified regions shown in the following images. Scale bars, 100 μm. (B2–6) High-magnification images. Arrows indicate the faint traces of sarcomere structure. Scale bars, 10 μm.

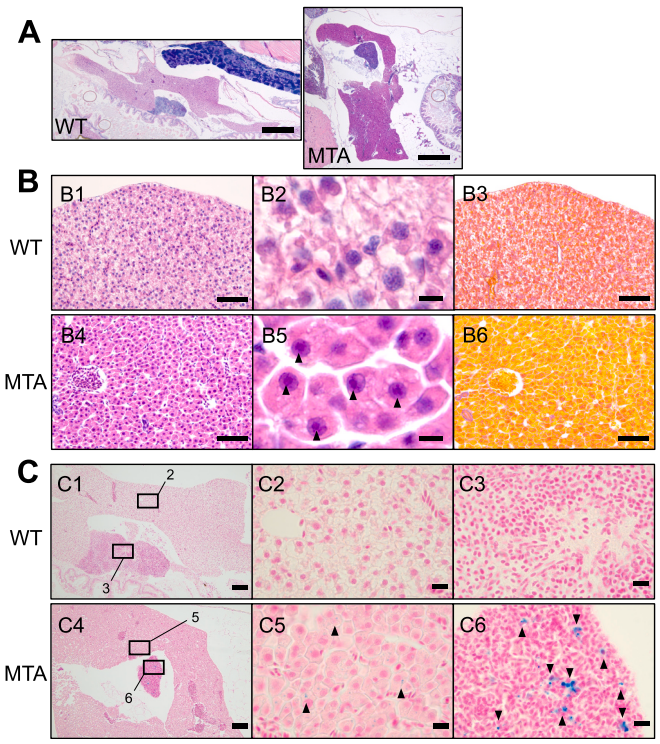

Fig. 6. Abnormal appearance of hepatocytes and iron depositions in the liver and spleen of the *slc25a20* mutant. (A) Representative images of the whole liver from hematoxylin and eosin (HE)-stained paraffin sections of the individuals. Scale bar, 0.5 mm. (B) Representative images of liver tissues from the wild-type fish (B1–3) and the mutant (B4–6). (B1, B4) Low-magnification images of the livers from HE-stained paraffin sections. Scale bars, 50 μm. (B2, B5) High-magnification images of hepatocytes. The back arrowheads indicate prominent nucleoli. Scale bars, 5 μm. (B3, B6) Images of azan-stained paraffin sections adjacent to those in B1 and B4. (C) Representative images of the liver and spleen from Prussian blue-stained paraffin sections of the wild-type fish (C1–3) and the mutant (C4–6). (C1, C4) Low-magnification images. Squares correspond to the magnified regions shown in the following images. Scale bars, 100 μm. (C2, C5) High-magnification images of the livers. Scale bars, 10 μm. (C3, C6) High-magnification images of the spleens. The back arrowheads indicate focal trace iron depositions. Scale bars, 10 μm.

resembling those found in cardiomyocytes, along with some eosin-negative vacuoles, within the muscle cells (Fig. 5 A6). Observation of the tail region near the trunk revealed that the majority of the mutant's muscle tissue exhibited normal sarcomere structure, but there was a marked increase in cell disruption toward the body surface (Fig. 5B). These findings show the skeletal muscle of the mutant exhibited lipid storage myopathy and cell degeneration.

One of the known symptoms of CACT deficiency is the accumulation of fat in hepatocytes, resulting in fatty liver, hepatomegaly, and liver fibrosis [2,3,11,25–28]. Therefore, we examined morphological abnormalities in the liver of the mutant (Fig. 6). There did not appear to be any particularly marked differences in organ size or shape between the wild-type fish and the mutant (Fig. 6A). The histological structure of the liver in the wild-type fish showed a typical picture of hepatocytes in zebrafish, with vacuolation that may be related to glycogen accumulation (Fig. 6B1, B2) [29]. On the other hand, the hepatocytes of the mutant not only showed no high vacuolation but also exhibited a bulky cellular morphology, widened intercellular spaces, homogeneous large nuclei and prominent nucleoli (Fig. 6B4, B5). We investigated fatty liver pathology in the liver of the mutant, and found no large oil droplet vacuoles, but a lot of small eosin-negative vacuoles in the hepatocytes that might be small lipid droplets (Fig. 6B5), and no significant fibrosis in the azan-stained tissue (Fig. 6B6). There is a report of iron deposition in the liver of a patient with CACT deficiency [19], so Prussian blue-stained sections were observed (Fig. 6C). No noticeable iron deposition was found in the liver and spleen of the wild-type fish (Fig. 6 C1—C3), but focal trace iron deposition was observed in the liver and large amounts were observed in the spleen of the mutant fish (Fig. 6C4—C6). These results indicate that, to varying degrees, the mutant liver showed similar abnormalities as the livers of patients with human CACT deficiency.

Histological examination of the mutant's kidneys and brain was performed, as cases of lipid accumulation in the renal tubules [14,25,27,28,30] and a case of moderate cortical volume loss in the brain [31] have been reported. However, no significant differences were observed compared to those of the wild-type fish. Based on these observations, despite some differences, the zebrafish *slc25a20* mutant produced in this study appears to have a homologous histopathology to human CACT deficiency.

4. Discussion

In this study, we generated a mutant zebrafish of the *slc25a20* gene to analyze its function in vivo. The *SLC25A20* gene encodes CACT [5–7], one of the factors in the carnitine cycle [8], and is an essential protein for energy production via β-oxidation in mitochondria [9]. Therefore, the loss of its function leads to severe consequences, and it is known that mutations in this gene in humans result in CACT deficiency, which manifests with severe symptoms shortly after birth [1–4]. The mutant zebrafish of the *slc25a20* generated in our study appears to be a useful disease model for this rare genetic disorder. The homozygous mutants exhibited significant lethality, with the majority dying before reaching maturity. Due to the analysis relying on a single, exceptionally rare

survivor, quantitative experiments such as qPCR or Western blotting to measure the amount of *slc25a20* RNA or protein levels are not feasible. Therefore, the conclusions that can be drawn remain limited. Off-target effects can occur in mutants generated with CRISPR/Cas9 [32], although the frequency may be low [33,34]. To address this, it would be beneficial to compare phenotypes across independently generated mutants to confirm consistency. While we did not analyze multiple mutant lines in zebrafish in this study, we did compare phenotypes between species - zebrafish and humans. The *slc25a20* mutant closely mimicked characteristic histopathology of the human disease, including fat accumulation in various tissues, cardiac hypertrophy, and degeneration of cardiomyocytes and skeletal muscle cells. Given the similarity in these phenotypes, we believe that any off-target effects are likely minimal. This study highlights the potential utility of the zebrafish model in future research on the pathogenesis and treatment of this rare disease.

The insertion mutation in exon 2 we introduced into the zebrafish *slc25a20* gene resulted in a frameshift, leading to the loss of approximately 250 amino acid residues at the C-terminal end of CACT, which accounts for 83 % of its total length. Assuming that the mRNA is spliced normally, the protein is presumed to lose most of its function due to the loss of multiple amino acid residues essential for transport activity [7,22], along with the deletion of 5 out of 6 transmembrane regions [5]. This speculation is supported by the fact that no CACT activity was detected in a fibroblast cell line derived from a skin biopsy of a patient with a frameshift mutation c.179del (p.Lys61fs) in the same exon 2 [27,35]. On the other hand, in patients with a frameshift mutation c.270delC (p.Phe91fs, alternative published notation: 306delC [1]), a small number of transcripts lacking the exon 3 containing the mutation existed [36]. However, even if splicing that skips exon 2 occurs in the zebrafish mutants, considering (1) the significant distortion of protein conformation due to the loss of 31 amino acid residues, (2) the expected rarity of abnormal transcripts [36], and (3) the similarity in phenotype between patients with the mutations p.Lys61fs or p.Phe91fs exhibiting severe neonatal-onset form [1,35,37] and the zebrafish mutants showing strong lethality before maturation, it is likely that the zebrafish mutant in this study may also significantly lose the activity of CACT.

To elucidate similarities and differences with the histopathology observed in human CACT deficiency, we analysed the tissues of the zebrafish mutant. While some patients with CACT deficiency develop hypertrophic cardiomyopathy [11,14,26,31], the ventricles of the zebrafish mutant also exhibited significant hypertrophy. Its cardiomyocytes were also clearly degenerated, and in addition to vacuoles, which appeared to be fatty accumulations as reported in the patient's cardiomyocytes [3,25–28,30,38], we found the particles with eosin cores, that may be related to small dark-brown granules observed in a patient [26]. These particles, also observed in the skeletal muscles, may represent lipid-filled vesicles with a nucleus composed of the long-chain acylcarnitine that is an amphiphilic chemical, accumulated excessively in cells due to defective CACT activity and causes toxicity for the heart and skeletal muscle [39–41]. In skeletal muscles of the zebrafish mutant, similar to observations in human patients with CACT deficiency, we observed lipid accumulation and degeneration of muscle cells, resembling findings of lipid storage myopathies or rhabdomyolysis [3,11,14,38]. We obtained observations of lipid accumulation and muscle cell degeneration, particularly in regions close to the body surface. This could be attributed to either (1) the inference from the fish's movement suggesting that muscles closer to the body surface experience greater rates of length expansion and contraction, thus consuming more energy, or (2) the anatomical feature that slow muscles, which have more mitochondria and undergo more β-oxidation than fast muscles, are distributed near the body surface in the centre of the torso in zebrafish [42]. In the zebrafish mutant, substantial accumulation of adipose tissue was observed in the subcutaneous and coelomic cavity regions. However, descriptions of similar pathological findings, such as the accumulation of subcutaneous or visceral fat, are not commonly reported in the diagnosis or autopsy of patients with CACT deficiency. Several reasons could explain this discrepancy. Firstly, many patients may not accumulate fat in the subcutaneous or body cavity regions due to their short lifespan [11]. Secondly, in patients with long-term survival, nutritional intake was strictly controlled, preventing excessive fat accumulation [11]. Alternatively, species differences may exist regarding the priority of sites where fat is stored. The third reason may be related to the observations that whereas no large oil droplet vacuoles were observed in the liver of the zebrafish mutant. Thus, the zebrafish *slc25a20* mutant we generated in this study is thought to have, albeit with some differences, a histopathology homologous to human CACT deficiency.

The zebrafish *slc25a20* mutant generated in this study might contribute to the improvement and development of treatments for CACT deficiency, a rare disorder. Patients with CACT deficiency typically rely on postnatal dietary interventions [2,26,43,44], including a high carbohydrate diet with restricted long-chain fat intake, as well as supplementation with triheptanoin [45] or medium-chain triglycerides (MCT) [46]. Beyond the optimization and enhancement of these dietary therapies, data regarding the debated cardiotoxicity of L-carnitine supplementation may also be obtained [1,11,47]. Furthermore, drug screening on the zebrafish mutant embryos prior to hatching may lead to the identification of compounds effective in ameliorating the pathology [48,49], potentially opening avenues for prenatal therapeutic interventions for CACT deficiency patients. The zebrafish *slc25a20* mutant exhibited strong lethality, with most individuals not surviving to maturity. While the specific timing of death – whether during the embryonic, juvenile or adult stage – remain unclear, this could be clarified by conducting genotyping at multiple time points. Additionally, examining histopathology at stages shortly before death may reveal the progression of tissue pathology in this zebrafish model of disease, potentially offering insights into the pathology progression of human CACT disease.

The *slc25a20* mutants used in this study exhibited a severe phenotype with high lethality, making detailed analysis challenging. In human CACT disease, in addition to the neonatal-onset type, which often results in death during the neonatal period, there is a later-onset type with milder symptoms, and several mutation sites are already known (e.g., p.Gly28Cys) [2,4,10,11]. Although somewhat challenging, it is possible to introduce site-specific mutations in zebrafish [50,51]. Therefore, our report that the zebrafish model closely mimics human CACT disease encourages the creation of zebrafish mutants with expected milder phenotypes. If mutants with milder phenotypes can be generated, it is anticipated that more detailed analyses will be more easily conducted.

Recent studies have revealed the involvement of the *slc25a20* gene in aging and cancer. Decreased expression of the *slc25a20* gene has been strongly correlated with muscle aging [52], suggesting its involvement in muscle aging as a master regulator of mitochondrial β-oxidation. Additionally, reduced expression of the *slc25a20* gene has been reported to promote the growth and metastasis of hepatocellular carcinoma [53] and the gene was identified as one of the hub genes in the progression of esophageal cancer [54], implying its tumor-suppressive role. In the hepatocytes of the zebrafish *slc25a20* mutant, we observed some features which may be related to the oncogenic process: large nuclei [55], prominent nucleoli [56] and iron deposition [57]. Such biological functions of *SLC25A20*, often overshadowed by the severe phenotype of CACT deficiency, could be elucidated through detailed analysis of seemingly healthy *slc25a20* heterozygous mutants, the utilization of homozygous mutants with reduced lethality through appropriate feeding and drugs supplementation, and generation and analysis of fish with the aforementioned mutations exhibiting milder phenotypes.

Funding

This work was supported by Takeda Science Foundation (HM), JSPS KAKENHI Grant Number JP 23790744 (HM), JSPS KAKENHI Grant Number JP 22484842 (HM), JSPS KAKENHI Grant Number JP 18955907 (HM), JSPS KAKENHI Grant Number JP 22 K07020 (RH),

MEXT Education and Research Organization Reform Project (21st Century Brodmann Areas Mapping Integrating Molecular and Functional Information) (RH), AMED Grant Number JP23gm1710010 (HM) and JP23gm1710001h0002 (ST), AMED Grant Number JP22gm6110028 (HM), AMED Grant Number JP20dm0107154 (HM), and JST [Moonshot R&D][Grant Number JPMJMS2024] (HM).

CRediT authorship contribution statement

Ryuichi Hishida: Writing – original draft, Investigation, Funding acquisition, Conceptualization. **Kohei Ishiguro:** Investigation. **Tomoyuki Yamanaka:** Investigation. **Shinya Toyokuni:** Writing – review & editing, Investigation, Funding acquisition. **Hideaki Matsui:** Writing – review & editing, Writing – original draft, Project administration, Methodology, Investigation, Funding acquisition, Conceptualization.

Declaration of competing interest

The authors declare no competing interests.

Data availability

Data will be made available on request.

Acknowledgements

We thank Nobuaki Misawa for technical assistance, Noriko Matsui and Shinano Kobayashi for fish maintenance and laboratory assistance.

References

[1] M. Rubio-Gozalbo, J.A. Bakker, H.R. Waterham, et al., Carnitine-acylcarnitine translocase deficiency, clinical, biochemical and genetic aspects, Mol. Asp. Med. 25 (5–6) (2004) 521–532, https://doi.org/10.1016/j.mam.2004.06.007.

[2] Vitoria I, Martín-Hernández E, Peña-Quintana L, et al. Carnitine-acylcarnitine translocase deficiency: experience with four cases in spain and review of the literature. Zschocke J, Baumgartner M, Morava E, et al. eds. JIMD Rep. 20 2015; 11–20; doi:https://doi.org/10.1007/8904_2014_382.

[3] X. Li, F. Zhao, Z. Zhao, et al., Neonatal sudden death caused by a novel heterozygous mutation in SLC25A20 gene: a case report and brief literature review, Legal Med. 54 (2022) 101990, https://doi.org/10.1016/j.legalmed.2021.101990.

[4] J.A. Morales Corado, C.U. Lee, G.M. Enns, Carnitine-acylcarnitine translocase deficiency, in: M.P. Adam, J. Feldman, G.M. Mirzaa, et al. (Eds.), GeneReviews®, University of Washington, Seattle: Seattle (WA), 2022.

[5] C. Indiveri, V. Iacobazzi, N. Giangregorio, et al., The mitochondrial carnitine carrier protein: cDNA cloning, primary structure and comparison with other mitochondrial transport proteins, Biochem. J. 321 (3) (1997) 713–719, https://doi.org/10.1042/bj3210713.

[6] J.J. Ruprecht, E.R.S. Kunji, The SLC25 mitochondrial carrier family: structure and mechanism, Trends Biochem. Sci. 45 (3) (2020) 244–258, https://doi.org/10.1016/j.tibs.2019.11.001.

[7] A. Tonazzi, N. Giangregorio, L. Console, et al., The mitochondrial carnitine acylcarnitine carrier (SLC25A20): molecular mechanisms of transport, role in redox sensing and interaction with drugs, Biomolecules 11 (4) (2021) 521, https://doi.org/10.3390/biom11040521.

[8] N. Longo, Amat Di San, C. Filippo, M. Pasquali, Disorders of carnitine transport and the carnitine cycle, Am. J. Med. Genet. C: Semin. Med. Genet. 142C (2) (2006) 77–85, https://doi.org/10.1002/ajmg.c.30087.

[9] R.J.A. Wanders, G. Visser, S. Ferdinandusse, et al., Mitochondrial fatty acid oxidation disorders: laboratory diagnosis, pathogenesis, and the complicated route to treatment, J. Lipid Atheroscler. 9 (3) (2020) 313–333, https://doi.org/10.12997/jla.2020.9.3.313.

[10] E. Lopriore, R.J.B.J. Gemke, N.M. Verhoeven, et al., Carnitine-acylcarnitine translocase deficiency: phenotype, residual enzyme activity and outcome, Eur. J. Pediatr. 160 (2) (2001) 101–104, https://doi.org/10.1007/s004310000644.

[11] B. Ryder, M. Inbar-Feigenberg, E. Glamuzina, et al., New insights into carnitine-acylcarnitine translocase deficiency from 23 cases: management challenges and potential therapeutic approaches, J. Inherit. Metab. Dis. 44 (4) (2021) 903–915, https://doi.org/10.1002/jimd.12371.

[12] M. Chen, Y. Cai, S. Li, et al., Late-onset carnitine–acylcarnitine translocase deficiency with SLC25A20 c.199-10T>G variation: case report and pathologic analysis of liver biopsy, Front. Pediatr. 8 (2020) 585646, https://doi.org/10.3389/fped.2020.585646.

[13] X. Li, J. Shen, One potential hotspot SLC25A20 gene variants in Chinese patients with carnitine-acylcarnitine translocase deficiency, Front. Pediatr. 10 (2022), https://doi.org/10.3389/fped.2022.1029004.

[14] N. Vatanavicharn, K. Yamada, Y. Aoyama, et al., Carnitine–acylcarnitine translocase deficiency: two neonatal cases with common splicing mutation and in vitro bezafibrate response, Brain and Development 37 (7) (2015) 698–703, https://doi.org/10.1016/j.braindev.2014.10.005.

[15] T. Otsuka, H. Matsui, Fish models for exploring mitochondrial dysfunction affecting neurodegenerative disorders, Int. J. Mol. Sci. 24 (8) (2023) 7079, https://doi.org/10.3390/ijms24087079.

[16] K. Fujii, K. Yamakawa, Y. Takeda, et al., Understanding the pathophysiology of acute critical illness: translational lessons from zebrafish models, Intensive Care Med. Exp. 12 (1) (2024) 8, https://doi.org/10.1186/s40635-024-00595-x.

[17] R.S. Angom, N.M.R. Nakka, Zebrafish as a model for cardiovascular and metabolic disease: the future of precision medicine, Biomedicines 12 (3) (2024) 693, https://doi.org/10.3390/biomedicines12030693.

[18] H. Matsui, A. Sugie, An optimized method for counting dopaminergic neurons in zebrafish. Kanungo J. ed, PLoS ONE 12 (9) (2017) e0184363, https://doi.org/10.1371/journal.pone.0184363.

[19] M. Jinek, K. Chylinski, I. Fonfara, et al., A programmable dual-RNA–guided DNA endonuclease in adaptive bacterial immunity, Science 337 (6096) (2012) 816–821, https://doi.org/10.1126/science.1225829.

[20] W.Y. Hwang, Y. Fu, D. Reyon, et al., Efficient genome editing in zebrafish using a CRISPR-Cas system, Nat. Biotechnol. 31 (3) (2013) 227–229, https://doi.org/10.1038/nbt.2501.

[21] H. Matsui, N. Kenmochi, K. Namikawa, Age- and α-Synuclein-dependent degeneration of dopamine and noradrenaline neurons in the annual killifish *Nothobranchius furzeri*, Cell Rep. 26 (7) (2019) 1727–1733.e6, https://doi.org/10.1016/j.celrep.2019.01.015.

[22] A. Pasquadibisceglie, V. Quadrotta, F. Polticelli, In silico analysis of the structural dynamics and substrate recognition determinants of the human mitochondrial carnitine/Acylcarnitine SLC25A20 transporter, Int. J. Mol. Sci. 24 (4) (2023) 3946, https://doi.org/10.3390/ijms24043946.

[23] D.M. Parichy, M.R. Elizondo, M.G. Mills, et al., Normal table of post-embryonic zebrafish development: staging by externally visible anatomy of the living fish, Dev. Dyn. Off. Publ. Am. Assoc. Anat. 238 (12) (2009) 2975, https://doi.org/10.1002/dvdy.22113.

[24] M. Haustein, T. Hannes, J. Trieschmann, et al., Excitation-contraction coupling in zebrafish ventricular myocardium is regulated by trans-Sarcolemmal Ca2+ influx and sarcoplasmic reticulum Ca2+ release, PLoS ONE 10 (5) (2015) e0125654, https://doi.org/10.1371/journal.pone.0125654.

[25] A.A.M. Morris, S.E. Olpin, M. Brivet, et al., A Patient with Carnitine-Acylcarnitine Translocase Deficiency with a Mild Phenotype, 1998.

[26] Y. Chinen, K. Yanagi, S. Nakamura, et al., A novel homozygous missense SLC25A20 mutation in three CACT-deficient patients: clinical and autopsy data, Hum. Genome Var. 7 (1) (2020) 1–4, https://doi.org/10.1038/s41439-020-0098-y.

[27] S.H. Korman, J.J. Pitt, A. Boneh, et al., A novel SLC25A20 splicing mutation in patients of different ethnic origin with neonatally lethal carnitine-acylcarnitine translocase (CACT) deficiency, Mol. Genet. Metab. 89 (4) (2006) 332–338, https://doi.org/10.1016/j.ymgme.2006.06.009.

[28] K. Choong, J.T. Clarke, E. Cutz, et al., Lethal cardiac tachyarrhythmia in a patient with neonatal carnitine-acylcarnitine translocase deficiency, Pediatr. Dev. Pathol. Off. J. Soc. Pediatr. Pathol. Paediatr. Pathol. Soc. 4 (6) (2001) 573–579, https://doi.org/10.1007/s10024001-0101-7.

[29] T.M. Bui-Nguyen, C.E. Baer, J.A. Lewis, et al., Dichlorvos exposure results in large scale disruption of energy metabolism in the liver of the zebrafish, *Danio rerio*, BMC Genomics 16 (1) (2015) 853, https://doi.org/10.1186/s12864-015-1941-2.

[30] D. Qiao, J. Jing, C. Zhang, et al., Sudden death with cardiac involvement in a neonate with carnitine-acylcarnitine translocase deficiency, Cardiovasc. Pathol. 107630 (2024), https://doi.org/10.1016/j.carpath.2024.107630.

[31] V. Iacobazzi, F. Invernizzi, S. Baratta, et al., Molecular and functional analysis of SLC25A20 mutations causing carnitine-acylcarnitine translocase deficiency, Hum. Mutat. 24 (4) (2004) 312–320, https://doi.org/10.1002/humu.20085.

[32] I. Höijer, A. Emmanouilidou, R. Östlund, et al., CRISPR-Cas9 induces large structural variants at on-target and off-target sites in vivo that segregate across generations, Nat. Commun. 13 (1) (2022) 627, https://doi.org/10.1038/s41467-022-28244-5.

[33] A. Hruscha, P. Krawitz, A. Rechenberg, et al., Efficient CRISPR/Cas9 genome editing with low off-target effects in zebrafish, Dev. Camb. Engl. 140 (24) (2013) 4982–4987, https://doi.org/10.1242/dev.099085.

[34] M.R. Mooney, E.E. Davis, N. Katsanis, Analysis of single nucleotide variants in CRISPR-Cas9 edited zebrafish exomes shows no evidence of off-target inflation, Front. Genet. 10 (2019) 949, https://doi.org/10.3389/fgene.2019.00949.

[35] C. Costa, J.M. Costa, A. Slama, et al., Mutational spectrum and DNA-based prenatal diagnosis in carnitine–acylcarnitine translocase deficiency, Mol. Genet. Metab. 78 (1) (2003) 68–73, https://doi.org/10.1016/S1096-7192(02)00205-6.

[36] B.Y.L. Hsu, V. Iacobazzi, Z. Wang, et al., Aberrant mRNA splicing associated with coding region mutations in children with carnitine-Acylcarnitine translocase deficiency, Mol. Genet. Metab. 74 (1–2) (2001) 248–255, https://doi.org/10.1006/mgme.2001.3235.

[37] B.B. Gürbüz, D.Y. Yılmaz, R.K. Özgül, et al., Clinical and molecular characteristics of carnitineacylcarnitine translocase deficiency with c.270delC and a novel c.408C>a variant, Turk. J. Pediatr. 63 (4) (2021) 691–696, https://doi.org/10.24953/turkjped.2021.04.017.

[38] B.-Z. Yang, J.M. Mallory, D.S. Roe, et al., Carnitine/Acylcarnitine translocase deficiency (neonatal phenotype): successful prenatal and postmortem diagnosis

associated with a novel mutation in a single family, Mol. Genet. Metab. 73 (1) (2001) 64–70, https://doi.org/10.1006/mgme.2001.3162.
[39] D. Bonnet, D. Martin, Pascale de Lonlay, et al., Arrhythmias and conduction defects as presenting symptoms of fatty acid oxidation disorders in children, Circulation 100 (22) (1999) 2248–2253, https://doi.org/10.1161/01.CIR.100.22.2248.
[40] P.B. Corr, M.H. Creer, K.A. Yamada, et al., Prophylaxis of early ventricular fibrillation by inhibition of acylcarnitine accumulation, J. Clin. Invest. 83 (3) (1989) 927–936, https://doi.org/10.1172/JCI113978.
[41] K.A. Yamada, E.M. Kanter, A. Newatia, Long-chain Acylcarnitine induces Ca2+ efflux from the sarcoplasmic reticulum, J. Cardiovasc. Pharmacol. 36 (1) (2000) 14–21, https://doi.org/10.1097/00005344-200007000-00002.
[42] S.H. Devoto, E. Melançon, J.S. Eisen, et al., Identification of separate slow and fast muscle precursor cells in vivo, prior to somite formation, Development 122 (11) (1996) 3371–3380, https://doi.org/10.1242/dev.122.11.3371.
[43] R.S.Y. Lee, C.W. Lam, C.K. Lai, et al., Carnitine-acylcarnitine translocase deficiency in three neonates presenting with rapid deterioration and cardiac arrest, Hong Kong Med J Xianggang Yi Xue Za Zhi 13 (1) (2007) 66–68.
[44] G. Pierre, A. Macdonald, G. Gray, et al., Prospective treatment in carnitine–acylcarnitine translocase deficiency, J. Inherit. Metab. Dis. 30 (5) (2007) 815, https://doi.org/10.1007/s10545-007-0518-x.
[45] S. Mahapatra, A. Ananth, N. Baugh, et al., Triheptanoin: a rescue therapy for cardiogenic shock in carnitine-acylcarnitine translocase deficiency, JIMD Rep. 39 (2017) 19–23, https://doi.org/10.1007/8904_2017_36.
[46] M.B. Gillingham, B. Scott, D. Elliott, et al., Metabolic control during exercise with and without medium-chain triglycerides (MCT) in children with long-chain 3-hydroxy acyl-CoA dehydrogenase (LCHAD) or trifunctional protein (TFP) deficiency, Mol. Genet. Metab. 89 (1) (2006) 58–63, https://doi.org/10.1016/j.ymgme.2006.06.004.
[47] C.R. Roe, H. Brunengraber, Anaplerotic treatment of long-chain fat oxidation disorders with triheptanoin: review of 15 years experience, Mol. Genet. Metab. 116 (4) (2015) 260–268, https://doi.org/10.1016/j.ymgme.2015.10.005.
[48] C.A. MacRae, R.T. Peterson, Zebrafish as tools for drug discovery, Nat. Rev. Drug Discov. 14 (2015) 721, https://doi.org/10.1038/nrd4627.
[49] E.E. Patton, L.I. Zon, D.M. Langenau, Zebrafish disease models in drug discovery: from preclinical modelling to clinical trials, Nat. Rev. Drug Discov. 20 (8) (2021) 611–628, https://doi.org/10.1038/s41573-021-00210-8.
[50] K. Petri, W. Zhang, J. Ma, et al., CRISPR prime editing with ribonucleoprotein complexes in zebrafish and primary human cells, Nat. Biotechnol. 40 (2) (2022) 189–193, https://doi.org/10.1038/s41587-021-00901-y.
[51] K. Hoshijima, M.J. Jurynec, D.J. Grunwald, Precise editing of the zebrafish genome made simple and efficient, Dev. Cell 36 (6) (2016) 654–667, https://doi.org/10.1016/j.devcel.2016.02.015.
[52] R. Fernando, A.V. Shindyapina, M. Ost, et al., Downregulation of mitochondrial metabolism is a driver for fast skeletal muscle loss during mouse aging, Commun. Biol. 6 (1) (2023) 1–11, https://doi.org/10.1038/s42003-023-05595-3.
[53] P. Yuan, J. Mu, Z. Wang, et al., Down-regulation of SLC25A20 promotes hepatocellular carcinoma growth and metastasis through suppression of fatty-acid oxidation, Cell Death Dis. 12 (4) (2021) 1–12, https://doi.org/10.1038/s41419-021-03648-1.
[54] F. Wang, L. Zhang, Y. Xu, et al., Comprehensive analysis and identification of key driver genes for distinguishing between esophageal adenocarcinoma and squamous cell carcinoma, Front. Cell. Dev. Biol. (2021) 9, https://doi.org/10.3389/fcell.2021.676156.
[55] E.G. Fischer, Nuclear morphology and the biology of cancer cells, Acta Cytol. 64 (6) (2020) 511–519, https://doi.org/10.1159/000508780.
[56] S. Kofuji, A. Hirayama, A.O. Eberhardt, et al., IMP dehydrogenase-2 drives aberrant nucleolar activity and promotes tumorigenesis in glioblastoma, Nat. Cell Biol. 21 (8) (2019) 1003–1014, https://doi.org/10.1038/s41556-019-0363-9.
[57] S. Toyokuni, I. Yanatori, Y. Kong, et al., Ferroptosis at the crossroads of infection, aging and cancer, Cancer Sci. 111 (8) (2020) 2665–2671, https://doi.org/10.1111/cas.14496.
[58] W. Li, A. Cowley, M. Uludag, et al., The EMBL-EBI bioinformatics web and programmatic tools framework, Nucleic Acids Res. 43 (W1) (2015) W580–W584, https://doi.org/10.1093/nar/gkv279.